White Rose Research Online

eprints@whiterose.ac.uk
https://eprints.whiterose.ac.uk
Universities of Leeds, Sheffield and York

Deposited via The University of Sheffield.

White Rose Research Online URL for this paper:
https://eprints.whiterose.ac.uk/id/eprint/204057/

Version: Published Version

Article:
Lister, S., Blanch, O.L., Fernandez, D.S. et al. (2023) A machinability assessment of the novel application of Field-Assisted Sintering Technology to Diffusion Bond (FAST-DB) and functionally grade dissimilar nickel-based superalloys. Metallurgical and Materials Transactions A, 54 (11). pp. 4396-4408. ISSN: 1073-5623

https://doi.org/10.1007/s11661-023-07173-y

Reuse
This article is distributed under the terms of the Creative Commons Attribution (CC BY) licence. This licence allows you to distribute, remix, tweak, and build upon the work, even commercially, as long as you credit the authors for the original work. More information and the full terms of the licence here:
https://creativecommons.org/licenses/

Takedown
If you consider content in White Rose Research Online to be in breach of UK law, please notify us by emailing eprints@whiterose.ac.uk including the URL of the record and the reason for the withdrawal request.

UNIVERSITY OF LEEDS
University of Sheffield
UNIVERSITY of York

ORIGINAL RESEARCH ARTICLE

A Machinability Assessment of the Novel Application of Field-Assisted Sintering Technology to Diffusion Bond (FAST-DB) and Functionally Grade Dissimilar Nickel-Based Superalloys

SAMUEL LISTER, OLIVER LEVANO BLANCH, DANIEL SUAREZ FERNANDEZ, JACOB POPE, GAVIN J BAXTER, SIMON BRAY, and MARTIN JACKSON

This work presents an alternative processing route to the conventional powder HIP—forge route for Nickel-based superalloys. Demonstrating how the field-assisted sintering technology (FAST) process can be exploited to successfully diffusion bond or functionally grade two or more Nickel-based superalloys from powder feedstock. The robustness of the process has been further demonstrated by the successful bonding of one alloy in powder form to another in the solid form. Chemical and microstructural analysis of the diffusion bond between the alloys is characterised, in both cases, with a short diffusion zone—in agreement with thermodynamic model predictions. A gradual transition in microhardness across the bond region was measured in all samples. A machinability assessment was also carried out through a simple face turning operation. Analysis of the cutting forces and machined surface shows signs of a directionality when machining across the bond region between two alloys, indicating that care must be taken when machining multi-alloy FAST-DB components.

https://doi.org/10.1007/s11661-023-07173-y
© The Author(s) 2023

I. INTRODUCTION

NICKEL-BASED superalloys are used in some of the most demanding components within gas turbine aero-engines owing to their elevated temperature strength and creep resistance.[1] As the drive towards net-zero gathers pace, there is a requirement for both manufacturing processes and component performance to be more efficient. Gas turbine components such as turbine disks and aerofoils are currently manufactured through either traditional cast/wrought processing or a powder metallurgy (PM) route such as Hot Isostatic Pressing(HIP) and isothermal forging, the microstructural evolution of which are discussed by Galpin.[2] In both cases, a large ingot is produced, forged and heat-treated before undergoing a significant amount of machining to the final part geometry. The buy-to-fly ratio of nickel components can be as low as 10:1 demonstrating that this method is highly inefficient with a vast amount of material being turned into waste machined swarf.

In recent years a number of near-net shape (NNS) advanced manufacturing techniques have emerged as potential replacement manufacturing routes, including additive manufacturing (AM) processes such as laser powder bed fusion (LBPF)[3] and directed energy deposition (DED).[4] The application of such processes for the aerospace sector was recently reviewed by Blakey-Milner *et al.*[5] Another potentially disruptive technology for the manufacturing of such components is Field-Assisted Sintering Technology (FAST), which has recently found increased applications for metals, despite being primarily a ceramic-processing technique since its invention.[6] FAST offers consolidation in the solid-state, similarly to HIP, with short processing times and direct heating in the material, a thorough discussion of the FAST technique is presented by Guillon *et al.*[7]

The implementation of FAST for industrial applications has been explored for titanium alloys throughout the past 10 years at The University of Sheffield, with shaped moulds and subsequent hot forging steps for automotive and aerospace applications being explored by Calvert *et al.*[8] Other researchers have investigated the use of FAST for nickel-based superalloys although

SAMUEL LISTER, OLIVER LEVANO BLANCH, DANIEL SUAREZ FERNANDEZ, JACOB POPE, GAVIN J. BAXTER, and MARTIN JACKSON are with the Department of Materials Science and Engineering, University of Sheffield, Sir Robert Hadfield Building, Mappin Street, Sheffield S1 3JD, UK. Contact e-mail: sam.lister@sheffield.ac.uk SIMON BRAY is with the Rolls-Royce plc, P.O. Box 31, Derby DE24 8BJ, UK
Manuscript submitted May 26, 2023; accepted August 10, 2023.
Article published online August 19, 2023

this work is quite limited. Ma *et al.*[9] investigated the effects of FAST processing parameters when consolidating IN718, *via* numerical simulation, finding that the main driving force of densification is plastic flow. Yan *et al.*[10] found that the phases present after sintering of IN718 at 1200 °C were similar to traditional wrought product, with a subsequent heat treatment further improving properties. Marshall *et al.*[11] compared the consolidation behaviour of a variation of the Rolls-Royce alloy RR1000 through HIP and FAST consolidation techniques and showed the microstructural evolution to be very similar through both routes. Yamanoglu *et al.*[12] studied the sintering characteristics and wear behaviour of a NNS nickel alloy, finding samples produced with a narrow particle size distribution (PSD) had a lower density. Borkar and Banerjee[13] found that sintering temperature played a more important role than pressure in determining the grain growth and mechanical properties when sintering elemental nickel powder. Tingaud *et al.*[14] processed a bimodal nickel-based superalloy powder, with the results showing that the consolidated samples inherited the heterogeneous structure of the starting powder, to give a mix of course and ultra-fine grains. Further discussion of the application to elemental and alloyed nickel can be found in the reviews by Ogunbiyi *et al.*[15] and Makena *et al.*[16]

Another method to improve the performance and efficiency of components is to use multi-materials or functionally graded materials, allowing site-specific properties to be produced. Traditionally, components are manufactured from one particular material or alloy despite requiring vastly different properties in sub-regions. Pope *et al.*[17] demonstrated that FAST could be used to manufacture titanium alloy components with dissimilar alloy regions through diffusion bonding (and termed FAST-DB), the deformation behaviour of such diffusion bonds has also been investigated by Levano Blanch *et al.*[18] Lin *et al.*[19] have researched applying this technique to nickel-based superalloys by bonding CM247LC powder with solid IN718 plate with a diffusion zone of 20 to 30 μm being measured and bond strength being equal to that of the lower strength alloy. A follow up study[20] investigated the bonding of solid CM247LC with solid IN718, with a slightly narrower diffusion bond of 20 μm being measured. After tensile testing the sample failed within the lower strength IN718 region and not at the bond interface, demonstrating excellent bond integrity. Zhang *et al.*[21] exploited a FAST furnace to join a solid single crystal nickel-based superalloy to a solid polycrystalline nickel-based superalloy without a graphite mould, which they termed pulsed current diffusion bonding. In the study they discovered that the pulsed current allows the heating to remain fairly localised at the bond interface, allowing the base metal to retain its structure. Interestingly, these authors did not explore the possibility of diffusion bonding two nickel-based superalloy powders *via* FAST.

Currently, to manufacture a multi-alloy nickel-based superalloy component separate monolithic parts must first be produced before being joined *via* one of a number of methods. The most common joining methods can be classified into several categories. For example, fusion welding processes such as Electron Beam Welding (EBW), Laser Beam Welding (LBW) and Tungsten Inert Gas (TIG) welding, the latter was investigated by Dye *et al.*,[22] where weldability maps for IN718 were developed by numerical analysis. Another category which has perhaps received the most attention for joining dissimilar nickel-based superalloys is friction welding processes such as Linear Friction Welding (LFW) and Inertia Friction Welding (IFW). Preuss *et al.*[23] first investigated the use of IFW for RR1000, performing metallurgical characterization in the as-welded and post-weld heat-treated (PWHT) conditions, discovering that small microstructural variations close to the weld zone led to significant differences in hardness. Preuss *et al.*[24] expanded the investigation of IFW from RR1000 to include superalloys IN718 and alloy 720Li. The joining of dissimilar nickel-based superalloys with IFW was explored for IN718/RR1000 by Daus *et al.*[25] finding that three different sets of welding parameters had little effect on weld microstructure and crack growth rate in high temperature fatigue testing. Senkov *et al.*[26] applied the IFW process to join LSHR, a PM alloy, and the directionally solidified Mar-M247 alloy. A comprehensive review of LFW and IFW for the joining of both similar and dissimilar nickel-based superalloys has been published by Chamanfar *et al.*.[27] Conventional diffusion bonding is another joining process which has been explored for IN718 by Zhang *et al.*,[28] with joint tensile strength being comparable to that of the parent material. Other methods make use of a filler material in the join between two components, traditionally brazing and more recently the Powder Interlayer Bonding (PIB) approach developed by Davies *et al.*[29] for titanium alloys. This technique has been applied to a monolithic nickel-based superalloy by Stanners *et al.*[30] which was then expanded on to join dissimilar alloys; RR1000, IN718 and a new generation superalloy (NGSA).[31] It was found that a region of increased hardness existed near the bond line in all bond combinations. Onuike and Bandyopadhyay[32] attempted to produce a bimetallic Ti-64 and IN718 structure using Laser Engineered Net Shaping (LENS) but encountered delamination at the bond interface due to thermal mismatch. They discovered that with the use of a third material as an interlayer, termed compositional bond layer (CBL), consisting of vanadium carbide mixed with the two alloys, it was possible to successfully build a crack-free structure. Whilst the joining techniques discussed here have been employed in various industrial applications, many are synonymous with disadvantages such as large heat-affected zones (HAZ), the requirement for a filler layer and/or a PWHT to relax residual stresses when joining precipitation-hardened superalloys with high γ'/γ'' content. Therefore, there is an appetite for more efficient joining processes with less detrimental effects to the microstructure and shorter processing routes.

In addition to the requirement for multi-alloy components there is also a desire amongst designers to functionally grade properties and/or composition, achieving a smooth transition rather than a sudden change in properties. FAST has been utilised to realise

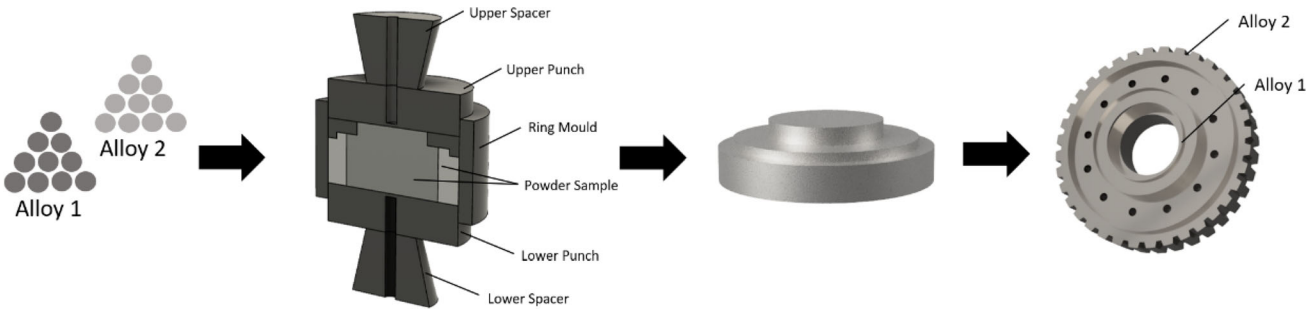

Fig. 1—A schematic showing how the authors envisage the FAST-DB process could be used for future industrial applications.

functionally graded materials (FGM) in combinations of metals and ceramics, highlighted in the recent exhaustive review by Charan *et al.*[33] although there is no mention of Ni-Ni FGM's. Popovich *et al.*[34] studied the use of AM to functionally grade IN718 by changing the laser source and scanning strategy, which created heterogeneity in grain size and microstructure. Ghorbanpour *et al.*[35] have also recently studied the fatigue behaviour of functionally graded IN718 produced *via* AM, demonstrating that there is considerable interest in development of FGM's for these alloys. This technique has been applied to many other alloy systems *via* AM, including joining Ni to Ti and steels, with varying levels of success as discussed by Reichardt *et al.*[36] However, there remains a gap in the literature for the production of Ni-Ni alloy FGM's which this study seeks to fill.

Whilst much focus is placed on the production of such multi-material components, their machinability is often overlooked, despite being a critical manufacturing step.[37] The machinability of nickel-based superalloys and the challenges they present have been discussed at length by both Ezugwu *et al.*[38] and Choudhury and El-Baradie.[39] Whilst an understanding of these notoriously difficult-to-machine monolithic superalloys has been developed over the years there are often other challenges to take into consideration when investigating machining multi-material components. Levano Blanch *et al.*[40] recently assessed the machinability of multi-material titanium alloy components made using FAST, highlighting that care must be taken when it comes to machining direction to control surface and subsurface damage. A comparative study for nickel-based superalloys has yet to be performed and this gap will be addressed here.

Therefore, despite there being a clear incentive to join alloys such as RR1000 and IN718 from the vast amounts of literature on the subject, there have been no reported attempts to do so *via* FAST. Furthermore, despite a small amount of research on this topic for other nickel-based superalloys, authors have overlooked the importance of assessing the machinability of such components. The machinability of multi-alloy nickel-based superalloy billets must be understood if the proposed FAST-DB manufacturing approach, shown schematically in Figure 1, is to be adopted by the aerospace industry and its full potential realised.

II. EXPERIMENTAL PROCEDURE

A. *Materials*

In this study two polycrystalline nickel-based superalloy powders of RR1000 and IN718 were used. RR1000 powder was provided by Rolls-Royce plc. with a pre-sieved particle size distribution (PSD) of 90 to 106 μm, in limited quantities. This powder was originally destined for use in additive manufacturing (AM), however it was oversized and surplus to requirements, due to the lower tolerance of the AM process to variable feedstock. An alternative source of RR1000 powder was used for the machining trial in Phase 3, with a much smaller PSD ($<$ 53 μm). The IN718 powder was purchased from Carpenter Additive, formerly LPW Technology, and had a PSD in a similar range to the second source of RR1000. The nominal composition of both alloys, as described by Hardy *et al.*[41] (RR1000) and Reed[1] (IN718), can be seen in Table I. Analysis of the PSD of these powders was conducted using a Malvern Mastersizer 3000 laser particle size analyser *via* the wet dispersion method. An average of 10 measurements for the Dx10, Dx50 and Dx90 were taken and used to calculate the relative span, shown in Table II.

The morphology of both powders (Phase 1 and 2) was analysed using an Olympus Bx51 optical microscope with Clemex Vision PE image analysis software. The software provides data on a range of powder features such as roundness, sphericity, aspect ratio and porosity. Figures 2(a) and (b) show the range and distribution of powder particles with varying roundness and sphericity for each alloy.

Comparing the morphologies of the two powders shows that RR1000 has a greater variation of powder particles with varying roundness and sphericity when compared to IN718, which has the highest density of powder particles within a much smaller region. Overall the range of roundness and sphericity values measured is quite similar for both alloys, although RR1000 consists of more particles with very low sphericity ($<$ 0.3).

B. *Experimental Approach/FAST Processing*

The FAST/SPS furnace used to consolidate and diffusion bond in this study was a FCT Systeme GmbH SPS Furnace Type HP D 25. The powder and/or solid feedstock were laid up in the required arrangement inside a 40 mm graphite mould. The mould was lined

with graphite foil to improve conductivity and aid sample removal post-sintering. Top and bottom graphite punches are inserted into the ring mould and the die is pre-pressed to 20 MPa in a hydraulic press. Following this the mould is placed in between the graphite supports and then secured inside the furnace between the top and bottom electrodes. An insulating graphite felt jacket was placed around the ring mould to reduce heat loss through radiation during processing. The electrodes then apply uniaxial pressure and a pulsed DC current which flows through the die and material, causing Joule heating and thus, sintering to occur.

The diffusion bonds produced in this study were classified into three phases; Phase 1—Powder to Powder, Phase 2—Powder to Solid and Phase 3: Machinability Assessment, as shown in Figure 3. The samples produced in Phase 1 consisted of a layer of RR1000 powder on the bottom, a layer of a functionally graded region of the two alloys and finally, a layer of IN718 on top. The functionally graded regions produced in Phase 1 were: no FGM region, 50 pct RR1000 50 pct IN718, 75 pct RR1000 25 pct IN718 and 25 pct RR1000 75 pct IN718.

Phase 2 of the study looked to investigate the bonding of IN718 powder onto a solid substrate produced from RR1000 also *via* FAST. The substrate was sectioned in half, perpendicular to the compression direction and then put back into the graphite mould, with a layer of IN718 powder on top of the bonding surface, these were then processed at the same conditions as in Phase 1.

For Phase 3 an additional diffusion bonded sample was made to allow the machinability of multi-material nickel superalloy components to be assessed. This sample was processed in a larger, 80 mm mould to facilitate easier sample clamping and allow a larger surface area to be machined. For the Phase 3 sample, the alloys were arranged so that the diffusion bond was parallel to the axial load using a 3D-printed polymer divider. The divider was removed before processing, this approach was necessary due to the requirement for the bond to be on the surface that was to be face machined, this would provide more data than an OD turning operation due to the limited sample height possible with FAST.

The key FAST processing parameters for each phase of the study are displayed in Table III. The power was reduced to 0 kW at the end of the dwell time for all samples, allowing the sample to cool inside the vessel relatively quickly. The average cooling rate from 1100 °C to 400 °C for each stage is shown in Table III.

The FAST processing parameters used in this study were based on optimal parameters previously used by Marshall *et al.*[11] in the same research group for nickel-based superalloys. Particularly, the dwell temperature of 1100 °C was selected due to being below the γ' solvus of RR1000 and hence, limit grain coarsening during processing. The aim of this study was to demonstrate the ability of the technique to diffusion bond dissimilar nickel-based superalloys in a range of forms, therefore no optimisation of processing parameters for microstructural or mechanical properties was considered at this stage.

C. *Analysis Techniques*

Each of the samples were sectioned perpendicular to the diffusion bond(s) and mounted in conductive Bakelite. Standard metallographic preparation techniques for nickel-based superalloys were used to prepare the samples for analysis. This included grinding with progressively finer SiC grit papers before a final polishing stage with a solution of 0.04 to 0.06 μm colloidal silica mixed with 30 pct hydrogen peroxide in a ratio of 9:1.

The microstructure of the diffusion bonds was analysed and imaged using a FEI Inspect F50 FEG-SEM in backscattered electron (BSE) mode, with an accelerating voltage of 20 kV. The elemental diffusion profile across the bond region was analysed using an Oxford Instruments Energy Dispersive X-Ray Spectrometry (X-EDS) system. Point line scans were taken, at x250 magnification, perpendicular to the bond with equidistant intervals of 40 μm and then 10 μm to allow a higher resolution of diffusion profile to be captured in the bond region.

Microhardness testing was conducted using a Struers Durascan 70 G5 automatic hardness indentation unit. Due to some samples containing a functionally graded region, a load of 2 kgf was applied, to allow a slightly larger indent to be made which was more likely to capture the mixture of the two alloys, rather than indenting a single alloy region of the composite which would be less representative of the bulk properties. The load was applied for 15 s for all indents in accordance with ASTM E384. In order to obtain as high a resolution as possible in the bond regions indents were made at a shallow angle across the bond. Each sample had at least two rows of 20 indents, with spacing of 300 μm, to provide an average measurement of the microhardness profile across the diffusion bond(s). A mosaic optical micrograph was taken of the indents on each sample using the Clemex software previously mentioned. This allowed the distance from the centre of each hardness indent to the bond interface to be measured using ImageJ software.[42]

The diffusion data taken from X-EDS was plotted using MATLAB software[43] to allow the diffusion region to be visualised. The data for the elemental concentrations of Fe and Co were chosen to be plotted as each exists solely in one alloy, allowing the diffusion zone to be easily distinguished. The raw data were plotted alongside a curve fit using the same method as described previously by Pope *et al.*,[17] which is based on the ideal mathematical solution for a diffusion couple with constant diffusion coefficient, solved using complementary error functions in agreement with Crank.[44] The thermodynamic modelling results were also plotted to allow an easy comparison between the measured, curve-fitted and modelled data to be made.

D. *Thermodynamic Modelling*

ThermoCalc 2020, a thermodynamic modelling software developed by Andersson *et al.*[45] and specifically the DICTRA diffusion module within the software, was used to model the diffusion profile between RR1000 and

Table I. The Nominal Composition in Wt Pct for Both RR1000 and IN718

Nominal Composition (Wt Pct)	Ni	Cr	Co	Mo	Nb	Al	Ti	Ta	Fe	Hf	C	B	Zr
RR1000	bal.	15.0	18.5	5.0	—	3.0	3.6	2.0	—	0.5	0.027	0.015	0.06
IN718	bal.	19.0	—	3.0	5.1	0.5	0.9	—	18.5	—	0.04	—	—

Table II. The Particle Size Distribution Measured for All of the Powders Used in this Study

Alloy	Dx(10) (μm)	Dx(50) (μm)	Dx(90) (μm)	Relative Span
RR1000 (Phase 1–2)	- pre-sieved 90 to 106 μm -			
RR1000 (Phase 3)	8.13	20.9	40.4	1.544
IN718 (Phase 1–3)	20.3	30.9	44.8	0.7933

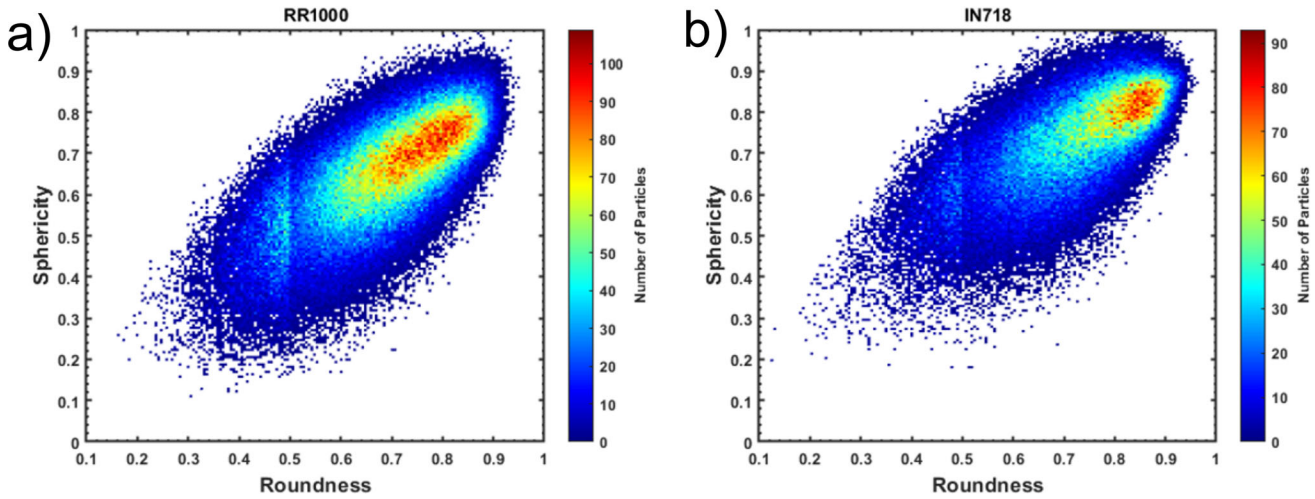

Fig. 2—(*a*) and (*b*) showing the distribution of the roundness and sphericity of RR1000 and IN718 powder particles.

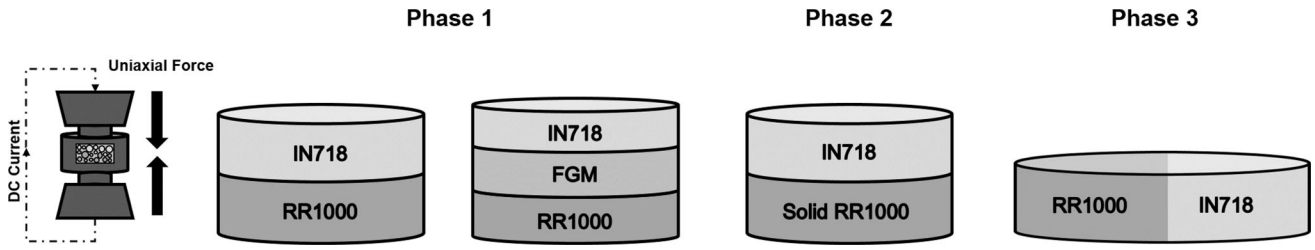

Fig. 3—A schematic showing the arrangement of RR1000 and IN718 in the mould for samples in each phase of the study.

IN718. This allowed a comparison to be made between the measured diffusion profile from the X-EDS data and the ideal case from the simulation. The diffusion bond was modelled as a 1D diffusion couple system with a 400 μm geometry. RR1000 was modelled on the left and IN718 on the right of the central interface at 200 μm, where a step change in the elemental composition of each alloy was applied. A double geometric grid type with point density of 0.97 and 1.03 as the lower and upper bounds was employed to provide a more refined grid around the interface, providing greater detail and computational accuracy.

The simulation was run at a dwell temperature of 1100 °C and a dwell time of 60 min, to model the parameters used in Phase 1 and Phase 2 of the FAST processing. TCNI10 thermodynamic and MOBNI5 mobility databases were used in the calculation. To limit the computational complexity and running time for the simulation, the FCC_L12 phase was selected only. This accounted for the γ and γ' phases, whilst other phases such as σ and γ'' play an important role in nickel-based superalloys, they are dissolved into solution at the dwell temperature and therefore were deemed not necessary to be included. The focus therefore was on

matrix to matrix diffusion of the two alloys, due to the low levels of precipitates present at the dwell temperature of 1100 °C. The homogenisation default solver, developed by Larsson and Höglund[46] was used to run the calculation.

E. *Machinability*

Phase 3 of the study consisted of a simple face turning machining trial, in which a WFL M100 MillTurn CNC machining centre was used to carry out the machining operation. The standard tungsten carbide tool insert used for this trial was a CNMG 12 04 08-mm H13A with a tool radius of 0.8 mm and manufactured by Sandivk. The forces generated during the machining operation were recorded with an acquisition rate of 40 kHz using a Kistler 9129 AA plate dynamometer, which was supporting the tool holder and connected directly to the machine arm. This allowed the forces experienced by the tool to be collected by piezoelectric sensors. The dynamometer signal was collected through a Kistler Type 5070 multi-channel charge amplifier, then the signal was sent to a Data Acquisition system (Kistler DAQ Type 5697A1).

The turning operation was performed at a constant RPM (G97) and the very conservative machining parameters used were; Feed Rate = 0.05 mm/rev, Depth-of-Cut (ap) = 0.05 mm, RPM = 137, with hocut-795b-eu coolant. The data recorded by the dynamometer was processed and reconstructed into a force map using a MATLAB script that has been developed by Levano Blanch *et al.*[40] for machining titanium alloys, but can be applied to a range of polycrystalline materials. The cutting force signal for the force in the z-direction was processed to remove noise and transformed from the time to the spatial domain to allow the force for a given point on the sample surface to be reconstructed in a map.

III. RESULTS AND DISCUSSION

A. *Phase 1 - Powder to Powder Bonding with Bond Line Perpendicular to FAST Axial Force*

1. *Bond microstructure*

The FAST-DB bond microstructure shown in Figure 4(a) shows a clear and defined diffusion bond between the two alloys, with the larger grains of RR1000 in the bottom half and the smaller grains of IN718 in the top half of the figure. In both alloys there is some local heterogeneity in grain size with some clusters of similar-sized grains observed. There are no obvious detrimental microstructural effects such as pores, cracks or intermetallic compounds in the bond region as a result of the FAST-DB process. The bond is relatively straight on a macroscopic level however there is some local irregularity—this is due to the two powders being layered on top of each other in the mould with the bond perpendicular to the axial force. Alternatively, a straighter bond may be achieved with the use of a powder divider which allows the two alloys to be placed inside the mould in their respective zones before the divider is removed leaving a relatively straight bond, parallel to the applied force. However, for this study the focus was on bonding the two alloys successfully in a range of conditions, rather than achieving a perfectly straight bond. Even with the use of a powder divider there will be some inherent irregularity in the bond due to the varying size and morphology of powder feedstock particles, as shown in Figures 2(a) and (b). There are no prior particle boundaries visible, further verifying that diffusion bonding has taken place.

Figures 4(d) and (e) show the FAST-DB diffusion bond for the sample containing a 50 pct RR1000, 50 pct IN718 functionally graded region. The composite sample demonstrates excellent diffusion bonding on two levels—firstly, on a macroscopic level between the bulk of RR1000/IN718 and the functionally graded region. Secondly, within the functionally graded region, it is apparent that successful bonding has occurred on a local scale between individual powder particles and grains. This confirms that FAST-DB can be used to create functionally graded nickel-nickel superalloy composites, with heterogeneous microstructures consisting of varying chemistry and grain size. This combination of chemistries and microstructures could unlock a new potential for nickel-based superalloys to be processed and functionally graded to achieve a unique combination of site-specific properties. In both of the other specimens with a composite mixed region, i.e., 25/75 pct and 75/25 pct, similar bonding behaviour was observed between both the bulk and the composite plus on a local level within the mixed region. Therefore, demonstrating that the microstructure and chemistry can be tailored by controlling the volume fraction of each alloy within the composite region, suggesting that the mechanical properties could also be manipulated in this way.

2. *Hardness profile across the bond*

Figures 5(a) through (d) shows the microhardness profiles across the diffusion bond for each of the samples in Phase 1. Figure 5(a) shows that there is a clear difference between the higher microhardness of RR1000 with an average of 429 HV with 95 pct confidence interval ± 2.950 HV and the much lower microhardness of IN718 which has an average of 247 HV with a 95 pct confidence interval of ± 1.479 HV. The lower hardness of IN718 may be due to the relatively quick cooling rates seen with FAST samples of this size (≈ 300 °C/min), which does not provide enough time for the reprecipitation of the γ'/γ'' precipitates as was seen after welding by Preuss *et al.*.[24] .On the other hand, the dwell temperature of 1100 °C is below the γ' solvus temperature in RR1000 and therefore although there may be some precipitate coarsening there isn't the same dissolution seen as in IN718. The microhardness profile shows a predictable transition from harder (RR1000) to softer (IN718) material, with the transition between the two alloys within a short region of 50 μm either side of the interface. This smooth transition is contrastingly different to the microhardness profiles seen when other joining techniques have been employed. For example, when Daus *et al.*[25] applied IFW to join RR1000 and

Table III. The Various Parameters Used During FAST Processing for Each Phase of the Study

	Heating Rate (°C/min)	Dwell Temperature (°C)	Dwell Time (min)	Pressure (MPa)	Ave. Cooling Rate (°C/min)
Phase 1	200	1100	60	41.4	306
Phase 2 Substrate	200	1100	15	41.4	311
Phase 2 Bonding	200	1100	60	41.4	333
Phase 3	42	1100	15	35	47

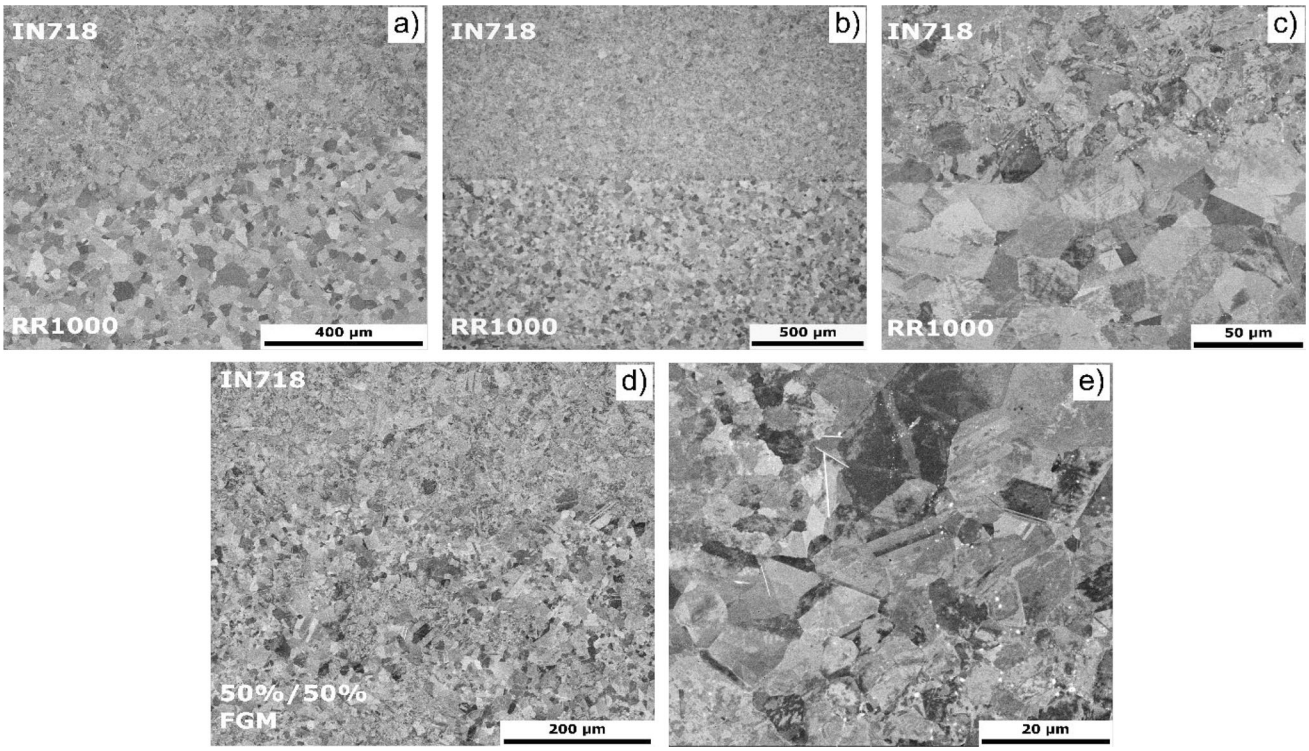

Fig. 4—(*a*) to (*e*) Backscattered electron images of the bond region in samples produced with (a) powder to powder, (*b*) and (*c*) powder to solid and (*d*) and (e) 50/50 functionally graded diffusion bonds.

IN718 there was an initial decrease in measured hardness before a peak at the weld line for RR1000, whereas a significant decrease in hardness from the bulk was measured approaching the weld line for IN718. The varying levels of hardness can be attributed to the HAZ which is several mm's in width either side of the weld line, where the thermal profile causes differing levels of precipitate dissolution and reprecipitation. With the FAST-DB technique, the same issues do not arise as the whole billet is exposed to the same thermal profile during processing rather than applying a local thermal profile as is the case with welding processes. Whilst the application of a PWHT allowed the IN718 hardness to recover, there still exists a peak hardness at the weld line which could have implications for residual stress. This increase in hardness at the bond interface was also measured by Stanners *et al.*[31] when bonding these two alloys *via* PIB. The hardness peak at the interface is not unique to the combination of RR1000 and IN718 as it was also observed by Senkov *et al.*[26] when bonding LSHR and Mar-M247, which they also attribute to the dissolution and reprecipitation of a finer dispersion of γ' at the weld line. The absence of a hardness peak at the bond in this study demonstrates that FAST-DB can be used as a joining process to produce subcomponent regions with different mechanical properties, whilst avoiding the issues seen with other joining techniques.

Figures 5(b) through (d) shows the microhardness profile across the functionally graded composite regions for the rest of the Phase 1 samples. The results show that there is considerable variation in the microhardness of the composite region, as the amount of plastic deformation will depend on the ratio of grains of each alloy indented. However, the average microhardness for each region follows the expected trend and lies in between that of the bulk alloys. For each of the three samples

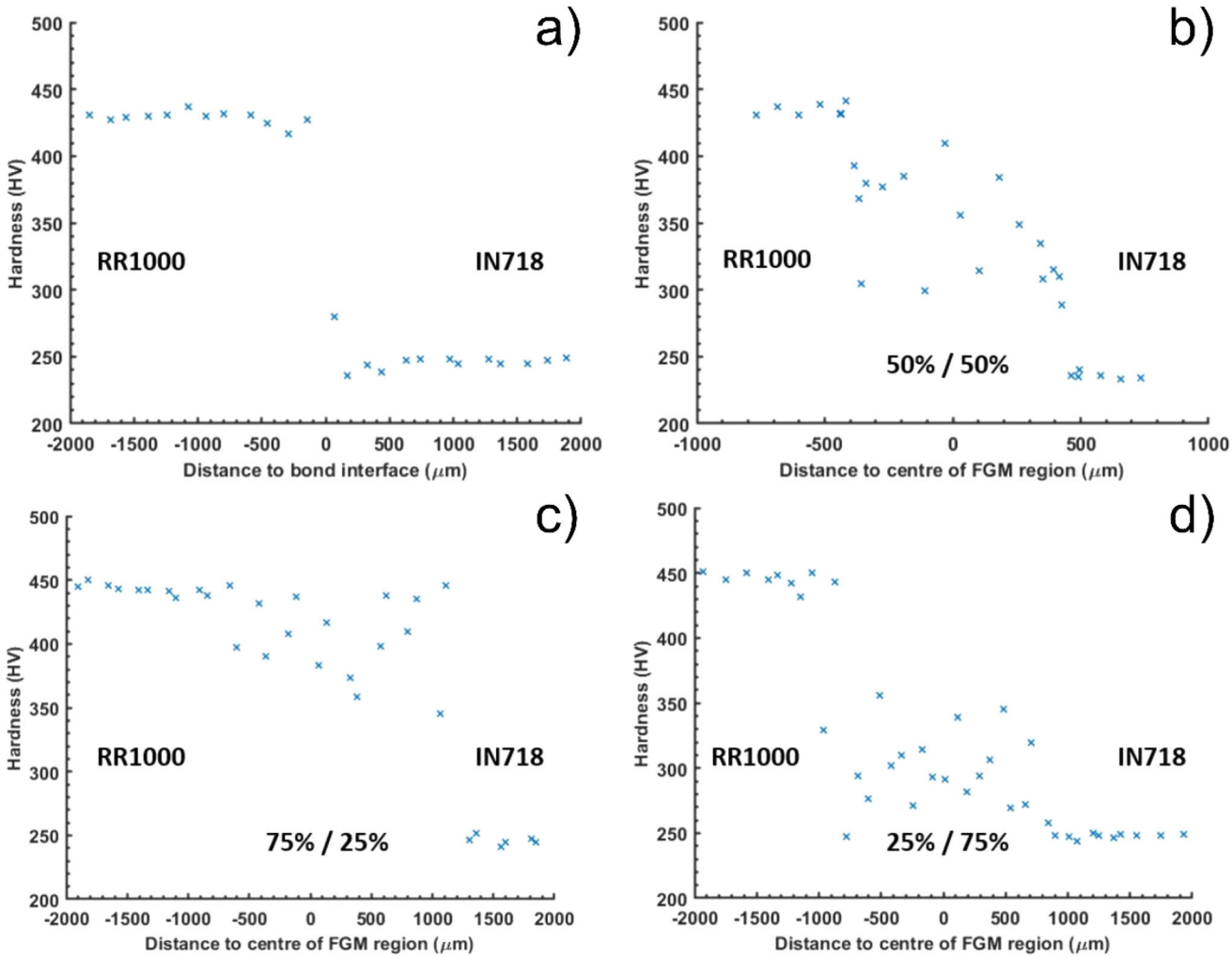

Fig. 5—(*a*) to (*d*): Measured microhardness profiles for powder to powder and functionally graded samples produced in Phase 1 of the study.

containing a composite mixed region, a theoretical rule-of-mixtures microhardness was calculated from the bulk hardness of each alloy and the volume fraction of each alloy. For the 50/50 composite this yielded a theoretical value of 335.19 HV, with the measured average composite microhardness being 345.71 HV. Similarly, for the 75/25 sample the theoretical value was calculated as 395.49 HV, with the measured average being 412.05 HV. Finally, for the 25/75 sample this was theoretically 297.16 HV and the average measured as 302.68 HV. These comparisons demonstrate the predictability and level of control which the FAST process can provide, with all 3 composites having an average microhardness within ± 17 HV of the calculated theoretical value.

3. *Measured and predicted elemental profile across FAST-DB interface*

Figures 6(a)and (b) display the measured X-EDS element concentrations across the diffusion bond region, with the raw data, curve-fitted and simulated values all compared for both cobalt (Co) and iron (Fe). These two alloying elements were chosen due to Co being exclusive to RR1000 and Fe exclusive to IN718. In Figure 6(a) a diffusion zone of around 50 μm either side of the bond was measured for Co, a slightly larger diffusion zone of around 60 μm was measured for Fe. In comparison, the ThermoCalc simulation clearly underestimates the level of diffusion to be in the region of 15 to 20 μm for both elements. This discrepancy can be attributed to assumptions made in the model, for example, the model simulates a 1D diffusion couple with a solid, perfectly straight interface. In reality, the powder to powder contacts along the bond will be uneven and some powder mixing may occur before consolidation occurs. Additionally, the nature of the powder to powder sintering may cause an increase in diffusion due to the enhanced level of Joule heating occurring at the particle to particle contacts. Both Yamanoglu *et al.*[12] and Borkar and Banerjee[13] have reported enhanced levels of diffusion due to the effects of pulsed current in the FAST process compared to conventional and direct current sintering. The presence of grain boundaries is also known to enhance diffusion, but is not considered in the DICTRA calculation. Furthermore, the simulation only considers diffusion that occurs during the

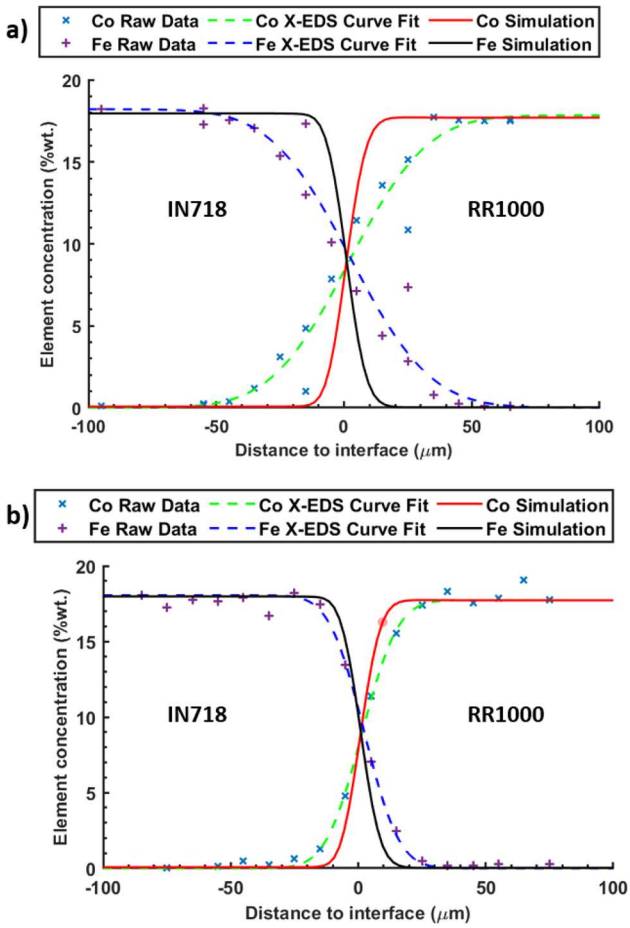

Fig. 6—(*a*), (*b*): Measured and predicted elemental profile across FAST-DB interface for (a) powder to powder and (b) powder to solid diffusion bonding.

60 min dwell at 1100 °C, in reality diffusion will also occur during the heating and cooling stages. The model is limited by these assumptions and underestimates the diffusion distance by 35 to 45 μm.

B. *Phase 2: Powder to Solid Bonding with Bond Perpendicular to FAST Axial Forces*

1. *Bond microstructure*

Figure 4(b) shows a low magnification BSE micrograph of the diffusion bond region for Phase 2 sample, with polished substrate. The lower region of the micrograph consists of the solid RR1000 substrate, with the upper region showing the IN718 powder which has been diffusion bonded—additively—to the substrate. This demonstrates the applicability of FAST as an additive manufacturing process, *e.g.,* for repair or coatings, in addition to other previously stated benefits. Figure 4(b) clearly shows a very straight diffusion bond with a clear, distinct difference between the two regions on the micro-scale. Similarly, to the Phase 1 samples, there are no defects or pores visible in the bond region, with the microstructure transitioning smoothly from that of IN718 to RR1000. Figure 4(c) shows a higher magnification image of the bond region.

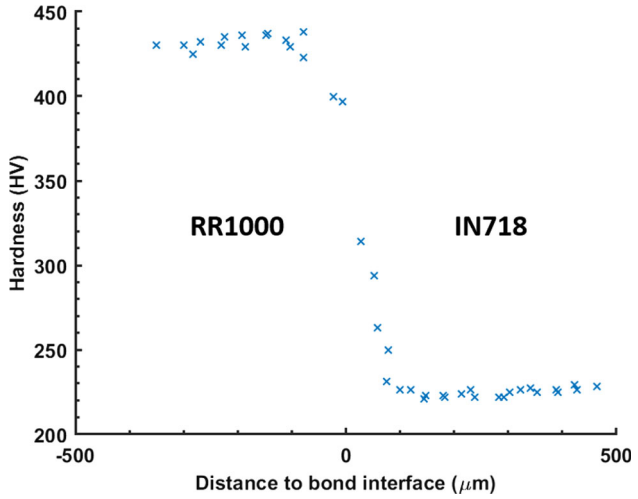

Fig. 7—Measured microhardness profile across the diffusion bond for powder to solid bonding.

2. *Hardness profile across the bond*

Figure 7 shows the microhardness profile across the diffusion bond, moving from RR1000 on the left to IN718 on the right, for the powder to solid bonded sample. The RR1000 substrate was polished to improve the quality of the substrate surface and promote diffusion bonding. The region of material with microhardness in between that of the bulk alloys is around 100 μm either side of the diffusion bond. This small region demonstrates the ability to join materials with vastly different mechanical properties with a very small interfacial region. The hardness profile follows a similar curve to that in Figure 5(a) for powder to powder bonding, although in the case of Phase 2, the region of transitioning microhardness is narrower. This is likely due to the same factors mentioned when discussing the measured elemental profile across the bond, with powder to solid bonding there is no opportunity for powder mixing to occur which artificially increases the width of the diffusion zone and hence transition in microhardness.

3. *Measured and predicted elemental profile across FAST-DB interface*

Figure 6(b) shows the elemental diffusion profile of Co and Fe, measured for the Phase 2 sample. The width of the diffusion zone is measured to be around 25 μm either side of the interface for Co and around 30 μm for Fe. In comparison to the values measured in Phase 1, it is clear that the diffusion zone is smaller. Similarly, the Phase 2 measured data are much closer to the simulated values, with the simulation underestimating by just 10 to 15 μm. This can be attributed to the fact that in Phase 2, a solid substrate is bonding with a powder. Therefore, this is closer to the modelled case, where a solid diffusion couple is assumed. Furthermore, no powder mixing between the two alloys can occur in the Phase 2 case during the setup and heating stages, thus reducing the potential for contamination and irregularity of the diffusion bond.

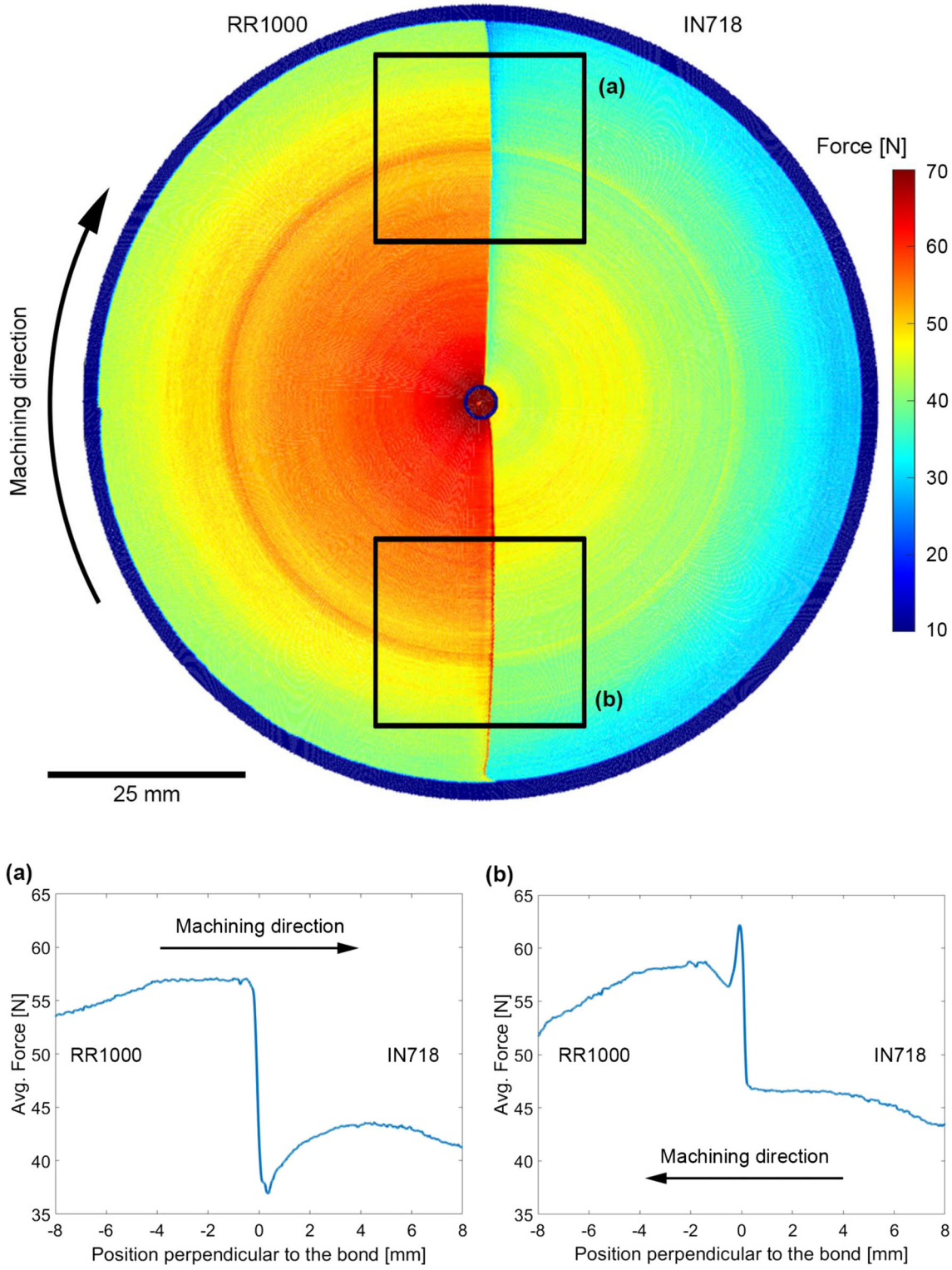

Fig. 8—Force feedback plot for a disc processed with FAST and made of IN718 and RR1000. The average machining force [in the *z*-direction (into the page)] recorded in the bond region is plotted when machining from (*a*) RR1000 to IN718 and (*b*) IN718 to RR1000 (as indicated on the force map).

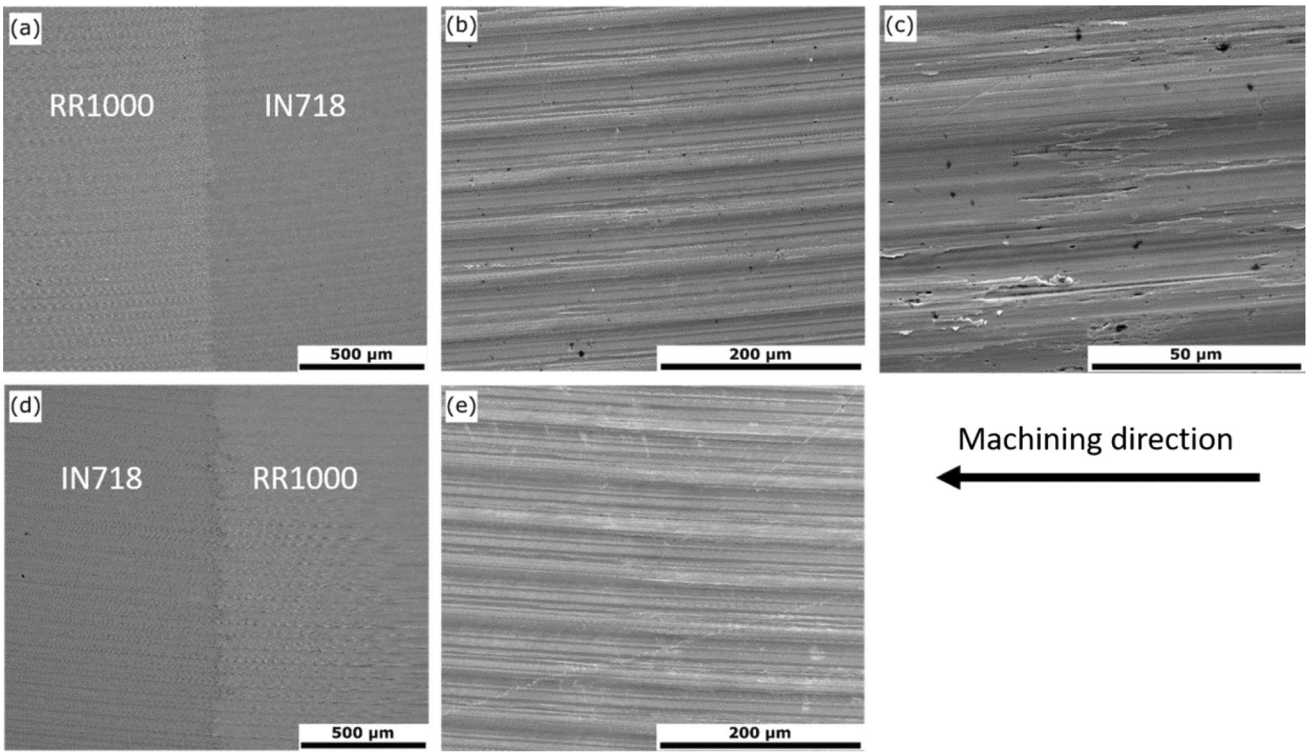

Fig. 9—(*a*) Backscatter electron micrograph (*b*), (*c*) secondary electron micrographs of bond region surface when machining from IN718 into RR1000. (*d*) Backscatter electron micrograph and (*e*) secondary electron micrograph of bond region surface when machining from RR1000 into IN718.

C. *Machinability of a Nickel Superalloy FAST-DB Billet*

The machinability of a FAST-DB billet processed from IN718 and RR1000 powder has been studied using a novel force feedback technique.[40] From the measured reaction forces during a turning operation, dissimilar alloys with different yield strengths can be located in the machined workpiece. Figure 8 shows the force feedback plot of the 80 mm diameter FAST billet. The reaction forces generated when machining the lower strength IN718 are lower than when machining RR1000 and the diffusion bond line can be clearly observed directly from force data. Interestingly, machining across the bond initially generates different forces depending on the cutting direction. To show the directionality effect in more detail, the average machining force across the bond has been plotted in a graph in Figure 8(a) and (b), using the method described by Levano Blanch *et al.*[40]. It is clear in both graphs that the decrease or increase of the forces is lower or higher than the average forces produced when machining the bulk material. When the direction of machining is from RR1000 into IN718, there is a local decrease in the cutting force before it returns to a steady state value for bulk IN718. Conversely, when machining from IN718 into RR1000 there is a rapid increase in the cutting force before a rapid decrease to a steady state value for bulk RR1000. This increase/decrease in cutting force is consistent every time the tool traverses across the bond region.

The surface finish at the bond region has also been analysed using scanning electron microscopy. Figure 9 shows the surface finish at the diffusion bond locations when machining from IN718 to RR1000 and when machining in the opposite direction. The backscattered electron micrograph in Figures 9(a), (d) shows the exact location of the bond for both directions. From these micrographs, it is not possible to distinguish significant differences between the two directions. However, at higher magnification [Figure 9(c)] it is possible to observe surface damage in the location of the bond when machining from IN718 to RR1000. The damage is characteristic of machining surface ''pick-up'' defects: the surface consists of smearing of IN718 material that has built-up at the tool cutting edge (built-up edge or BUE). Clearly the lower strength IN718 is depositing onto the surface as the tool abruptly traverses into the higher strength RR1000. Such deposition or smearing of the IN718 BUE from the tool (when cutting into the RR1000) onto the surface correlates with the peak force observed in Figure 8(b). In the opposing machining direction, no such surface defects are observed. Similar smearing and surface tear characteristics have been observed in IN718 previously by M'Saoubi *et al.*.[47]

From Figures 8 and 9, it is clear that the direction when cutting a dissimilar nickel-based superalloy billet has an influence on the final surface quality and the forces generated at the bond region. Other researchers have also seen an effect on the machining direction and the forces generated. Ullah *et al.*[48] machined multiple combinations of alloys and recorded the forces required to machine these components. The results presented in their work showed that the forces in the bond were lower when machining

from a lower to a higher strength material, contrary to the results in Figure 8. The different behaviour of the forces recorded could be related to the types of metals bonded together and the technique used for this. In the study by Ullah *et al.*[48], the metals were joined using inertia friction welding (IFW), which tends to create heat-affected zones (HAZ) on the order of millimetres. In our study, the alloys are bonded using FAST, which creates a diffusion bond in the order of the microns, as shown in Figure 6. Levano Blanch *et al.*[40] observed that when machining from a lower strength to a higher strength titanium alloy, a peak force and damage was observed at the bond, which agrees with the results presented in this work. It is thought that this peak force is caused by the abrupt change of material strength and resistance to deformation. This causes the tool to initially impact against a harder material and "wipe off" any accumulated built-up edge from the tool cutting edge onto the workpiece surface.

IV. CONCLUSIONS

The FAST-DB approach has been successfully applied to diffusion bond two nickel-based superalloy powders, RR1000 and IN718. This manufacturing approach has also been expanded to produce nickel-nickel superalloy functionally graded composites, demonstrating the potential to tailor properties in site-specific regions. It has also been demonstrated that FAST can be exploited to bond nickel-based superalloy powder to a solid nickel-based superalloy substrate, essentially an additive technique. In all cases, a gradual transition in microhardness and a predictable change in chemical composition with a small diffusion zone was measured across the bond.

An assessment of the machinability indicated that care must be taken during the machining of nickel-based superalloy FAST-DB billets and components as some directionality is observed in the measured forces and depositing of (IN718) built-up edge from the tool cutting edge onto the workpiece surface when machining from IN718 to RR1000 was seen. No surface defects are observed when machining from RR1000 to IN718.

ACKNOWLEDGMENTS

The authors would like to thank members of the Industrial Training Programme project for initial work and characterisation; Dominic Southall, Shiv Unka, Kristopher Price and Felix Mundanmany. Thanks also to Christos Argyrakis and Kyle Marshall from Rolls-Royce plc. for useful discussions and technical support with ThermoCalc and microscopy.

FUNDING

This work was supported by Rolls-Royce plc., Science Foundation Ireland (18/EPSRC-CDT/3584) and the Engineering and Physical Sciences Research Council UK (EP/S022635/1). We acknowledge the FAST/SPS capability as part of the Henry Royce Institute (EP/R00661X/1).

CONFLICT OF INTEREST

On behalf of all authors, the corresponding author states that there is no conflict of interest.

OPEN ACCESS

This article is licensed under a Creative Commons Attribution 4.0 International License, which permits use, sharing, adaptation, distribution and reproduction in any medium or format, as long as you give appropriate credit to the original author(s) and the source, provide a link to the Creative Commons licence, and indicate if changes were made. The images or other third party material in this article are included in the article's Creative Commons licence, unless indicated otherwise in a credit line to the material. If material is not included in the article's Creative Commons licence and your intended use is not permitted by statutory regulation or exceeds the permitted use, you will need to obtain permission directly from the copyright holder. To view a copy of this licence, visit http://creativecommons.org/licenses/by/4.0/.

REFERENCES

1. R.C. Reed: *The Superalloys Fundamentals and Applications*, vol. 9780521859, Cambridge University Press, Cambridge, 2006.
2. S.J. Galpin: *Mater. Sci. Technol.*, 2022, https://doi.org/10.1080/02670836.2022.2069332.
3. O. Adegoke, J. Andersson, H. Brodin, and R. Pederson: *Metals (Basel)*, 2020, vol. 10, pp. 1–26.
4. A.N. Jinoop, C.P. Paul, and K.S. Bindra: *Proc. Inst. Mech. Eng. Part L*, 2019, vol. 233, pp. 2376–400.
5. B. Blakey-Milner, P. Gradl, G. Snedden, M. Brooks, J. Pitot, E. Lopez, M. Leary, F. Berto, and A. Du Plessis: *Mater. Des.*, 2021, vol. 209, p. 110008.
6. M. Bram, A.M. Laptev, T.P. Mishra, K. Nur, M. Kindelmann, M. Ihrig, J.G. Pereira da Silva, R. Steinert, H.P. Buchkremer, A. Litnovsky, F. Klein, J. Gonzalez-Julian, and O. Guillon: *Adv. Eng. Mater.*, 2020, https://doi.org/10.1002/adem.202000051.
7. O. Guillon, J. Gonzalez-Julian, B. Dargatz, T. Kessel, G. Schierning, J. Räthel, and M. Herrmann: *Adv. Eng. Mater.*, 2014, vol. 16, pp. 830–49.
8. E. Calvert, B. Wynne, N. Weston, A. Tudball, and M. Jackson: *J. Mater. Process. Technol.*, 2018, vol. 254, pp. 158–70.
9. L. Ma, Z. Zhang, B. Meng, and M. Wan: *Materials (Basel)*, 2021, vol. 14, p. 2546.
10. S. Yan, Q. Wang, X. Chen, C. Zhang, and G. Cui: *Vacuum*, 2019, vol. 163, pp. 194–203.
11. K. Marshall, P. Schillinger, N. Weston, M. Epler, and M. Jackson: *Adv. Ind. Manuf. Eng.*, 2022, https://doi.org/10.2139/ssrn.4127787.
12. R. Yamanoglu, W. Bradbury, E. Karakulak, E.A. Olevsky, and R.M. German: *Powder Metall.*, 2014, vol. 57, pp. 380–86.
13. T. Borkar and R. Banerjee: *Mater. Sci. Eng. A*, 2014, vol. 618, pp. 176–81.
14. D. Tingaud, P. Jenei, A. Krawczynska, F. Mompiou, J. Gubicza, and G. Dirras: *Mater. Charact.*, 2015, vol. 99, pp. 118–27.

15. O.F. Ogunbiyi, T. Jamiru, E.R. Sadiku, O.T. Adesina, L. Beneke, and T.A. Adegbola: *Procedia Manuf.*, 2019, vol. 35, pp. 1324–29.
16. I.M. Makena, M.B. Shongwe, M.M. Ramakokovhu, and M.L. Lethabane: in *Proceedings of the World Congress on Engineering*, 2017, vol. 2, pp. 922–27.
17. J.J. Pope, E.L. Calvert, N.S. Weston, and M. Jackson: *J. Mater. Process. Technol.*, 2019, vol. 269, pp. 200–07.
18. O. Levano Blanch, D. Lunt, G.J. Baxter, and M. Jackson: *Metall. Mater. Trans. A*, 2021, vol. 52A, pp. 3064–82. https://doi.org/10.1007/s11661-021-06301-w.
19. C.I. Lin, S.J. Niuman, A.K. Kulkarni, D.S. King, J. Singh, and N. Yamamoto: *Metall. Mater. Trans. A*, 2020, vol. 51A, pp. 1353–66.
20. C.I. Lin, N. Yamamoto, D.S. King, and J. Singh: *Metall. Mater. Trans. A*, 2021, vol. 52A, pp. 2149–54.
21. B. Zhang, C. Chen, Z. Cai, H. Tian, J. Hou, L. Chai, Y. Lv, and J. He: *J. Alloys Compd.*, 2022, vol. 890, p. 161681.
22. D. Dye, O. Hunziker, and R.C. Reed: *Acta Mater.*, 2001, vol. 49, pp. 683–97.
23. M. Preuss, P.J. Withers, J.W.L. Pang, and G.J. Baxter: *Metall. Mater. Trans. A*, 2002, vol. 33A, pp. 3215–25.
24. M. Preuss, P.J. Withers, and G.J. Baxter: *Mater. Sci. Eng. A*, 2006, vol. 437, pp. 38–45.
25. F. Daus, H.Y. Li, G. Baxter, S. Bray, and P. Bowen: *Mater. Sci. Technol.*, 2007, vol. 23, pp. 1424–32.
26. O.N. Senkov, D.W. Mahaffey, S.L. Semiatin, and C. Woodward: *Metall. Mater. Trans. A*, 2014, vol. 45, pp. 5545–61.
27. A. Chamanfar, M. Jahazi, and J. Cormier: *Metall. Mater. Trans. A*, 2015, vol. 46A, pp. 1639–69.
28. G. Zhang, R.S. Chandel, and H.P. Seow: *Sci. Technol. Weld. Join.*, 2001, vol. 6, pp. 235–39.
29. P. Davies, A. Johal, H. Davies, and S. Marchisio: *Int. J. Adv. Manuf. Technol.*, 2019, vol. 103, pp. 441–52.
30. O. Stanners, S. John, H.M. Davies, I. Watkins, and S. Marchisio: *Materials (Basel)*, 2020, vol. 13, pp. 1–3.
31. O. Stanners, J. Russell, S. John, H.M. Davies, and S. Marchisio: *Materials (Basel)*, 2021, https://doi.org/10.3390/ma14082029.
32. B. Onuike and A. Bandyopadhyay: *Addit. Manuf.*, 2018, vol. 22, pp. 844–51.
33. M. SaiCharan, A.K. Naik, N. Kota, T. Laha, and S. Roy: *Int. Mater. Rev.*, 2022, https://doi.org/10.1080/09506608.2022.2026863.
34. V.A. Popovich, E.V. Borisov, A.A. Popovich, V.S. Sufiiarov, D.V. Masaylo, and L. Alzina: *Mater. Des.*, 2017, vol. 114, pp. 441–9.
35. S. Ghorbanpour, K. Deshmukh, S. Sahu, T. Riemslag, E. Reinton, E. Borisov, A. Popovich, V. Bertolo, Q. Jiang, M. Terol, M. Knezevic, and V. Popovich: *J. Mater. Process. Tech.*, 2022, vol. 306, p. 117573.
36. A. Reichardt, A.A. Shapiro, R. Otis, R.P. Dillon, J.P. Borgonia, B.W. McEnerney, P. Hosemann, and A.M. Beese: *Int. Mater. Rev.*, 2021, vol. 66, pp. 1–29.
37. G. Kappmeyer, C. Hubig, M. Hardy, M. Witty, and M. Busch: *Procedia CIRP*, 2012, vol. 1, pp. 28–43.
38. E.O. Ezugwu, Z.M. Wang, and A.R. Machado: *J. Mater. Process. Technol.*, 1998, vol. 86, pp. 1–6.
39. I.A. Choudhury and M.A. El-Baradie: *J. Mater. Process. Technol.*, 1998, vol. 300, pp. 278–84.
40. O. Levano Blanch, D. Suárez Fernández, A. Graves, and M. Jackson: *Materials (Basel)*, 2022, https://doi.org/10.3390/ma15093237.
41. M.C. Hardy, C. Argyrakis, H.S. Kitaguchi, A.S. Wilson, R.C. Buckingham, K. Severs, S. Yu, C. Jackson, E.J. Pickering, S.C.H. Llewelyn, C. Papadaki, K.A. Christofidou, P.M. Mignanelli, A. Evans, D.J. Child, H.Y. Li, N.G. Jones, C.M.F. Rae, P. Bowen, and H.J. Stone: Superalloys 2020—Proceedings of the 14th International Symposium on Superalloys (*Minerals, Metals and Materials Series)*, Springer, 2020, pp. 19–30.
42. C.A. Schneider, W.S. Rasband, and K.W. Eliceiri: *Nat. Methods*, 2012, vol. 9, pp. 671–75.
43. The MathWorks Inc. MATLAB version 9.4 (2018a), 2018.
44. J. Crank: *Methods of Solution When The Diffusion Coefficient Is Constant*, Oxford, 1955.
45. J.O. Andersson, T. Helander, L. Höglund, P. Shi, and B. Sundman: *Calphad Comput. Coupling Phase Diagr. Thermochem.*, 2002, vol. 26, pp. 273–312.
46. H. Larsson and L. Höglund: *Calphad Comput. Coupling Phase Diagr. Thermochem.*, 2009, vol. 33, pp. 495–501.
47. R. M'Saoubi, T. Larsson, J. Outeiro, Y. Guo, S. Suslov, C. Saldana, and S. Chandrasekar: *CIRP Ann. Manuf. Technol.*, 2012, vol. 61, pp. 99–102.
48. A.M.M.S. Ullah: *J. Manuf. Mater. Process.*, 2018, vol. 2, pp. 1–22. https://doi.org/10.3390/jmmp2040068.

Publisher's Note Springer Nature remains neutral with regard to jurisdictional claims in published maps and institutional affiliations.